ISSN 1063-7826, Semiconductors, 2019, Vol. 53, No. 11, pp. 1465–1471. © Pleiades Publishing, Ltd., 2019.
Russian Text © The Author(s), 2019, published in Fizika i Tekhnika Poluprovodnikov, 2019, Vol. 53, No. 11, pp. 1505–1511.

SURFACES, INTERFACES, AND THIN FILMS

Structure and Electrical Properties of $(ZnO/SiO_2)_{25}$ Thin Films

M. N. Volochaev[a], Yu. E. Kalinin[b], M. A. Kashirin[b], V. A. Makagonov[b,*], S. Yu. Pankov[b], and V. V. Bassarab[b]

[a] *Kirensky Institute of Physics, Krasnoyarsk Scientific Center, Siberian Branch, Russian Academy of Sciences, Krasnoyarsk, 660036 Russia*

[b] *Voronezh State Technical University, Voronezh, 394026 Russia*

**e-mail: vlad_makagonov@mail.ru*

Received June 4, 2019; revised June 25, 2019; accepted June 25, 2019

Abstract—$(ZnO/SiO_2)_{25}$ thin-film multilayers consisting of nanocrystalline ZnO layers and amorphous SiO_2 spacers with a bilayer thickness from 6 to 10 nm are synthesized in a single deposition process. An analysis of the temperature dependences of the electrical resistivity of $(ZnO/SiO_2)_{25}$ thin films shows that, in the temperature range of 77–300 K, the dominant conductivity mechanism successively changes from hopping conductivity with a variable hopping length in a narrow energy band near the Fermi level at temperatures of 77–250 K to thermally activated impurity conductivity around room temperature. Using the obtained temperature dependences of the electrical resistivity, the effective density of localized states at the Fermi level and the activation energy of impurity levels are estimated. The effect of heat treatment on the structure and electrical properties of the synthesized films is examined. It is established that in $(ZnO/SiO_2)_{25}$ thin-film systems at temperatures of 580–600°C, the ZnO and SiO_2 layers chemically interact, which is accompanied by destruction of the multilayer structure and formation of the Zn_2SiO_4 compound with a tetragonal structure (sp. gr. I-42*d*).

Keywords: thin films, multilayers, oxide semiconductors, hopping conductivity, thermal stability

DOI: 10.1134/S106378261911023X

1. INRODUCTION

Zinc-oxide (ZnO) thin films exhibit a combination of properties important for application, including transparency in the visible electromagnetic-radiation range and low electrical resistance, which is facilitated by their wide band gap and the formation of nonstoichiometric compositions or the embedding of corresponding dopants [1–3]. The applicability of ZnO thin films depends not only on their optical and electrical properties; in addition, these parameters should be combined with stability against the effect of environmental factors, abrasion resistance, low electron work function, compatibility with a substrate, and other requirements for thin films of transparent semiconductors, depending on the area of their application.

The properties of zinc oxide and compounds based on it are determined primarily by the presence of oxygen vacancies, the number of which can be controlled by either introducing oxygen during synthesis of the material or heat treatment of the films in an oxidizing atmosphere [4]. Secondly, the properties are determined by the need for controlling the structural (amorphous or crystalline) state, which is achieved via the embedding of special amorphizers (Sn, Si, or other dopants) [4].

These two approaches can be combined in a joint vacuum deposition technique. Thus, in [5], $(SiO_2)_x(ZnO)_{100-x}$ (SZO) thin films with $x = 2$, 3, 4, and 5 mass % were obtained by the RF magnetron sputtering of ZnO and SiO_2 targets. It was found that the lowest resistivity (4.5×10^{-3} Ω cm) is obtained in the film with $x = 2$ mass % Si. This film exhibited a high (~85%) optical transparency in the visible wavelength range, which was facilitated by a band gap of more than 3.4 eV and a high (2.1) refractive index. The electrical resistivity of this film after annealing for 30 min at 300°C in vacuum reached 10^{-3} Ω cm, which is comparable with tin-doped indium oxide (ITO) films [6]. Consequently, SZO films are promising for application as alternative film materials for transparent electronics.

Recently, it was proposed that multilayer heterostructures consisting of oxide semiconductor layers be used as the channels of thin-film transistors (TFTs) [7–9]. Interest in such structures is due to the fact that, despite the intense use of wide-gap amorphous oxide semiconductors and solid solutions based on them as TFT channels, the instability and short life of the operating characteristics in single-layer TFT channels due to different conditions (temperature, bias, and illumination) are key problems in the application

of transparent conducting oxides. This instability is related to oxygen vacancies. At the same time, it is well-known that carriers in transparent oxide semiconductors are provided by oxygen defects and the density of oxygen vacancies determines the electrical properties of oxide semiconductors. Thus, one has to choose between operation stability and working characteristics. In addition, available TFT-channel materials do not meet the requirements for the operation speed, switching time, and carrier mobility.

This situation can be resolved by fabricating bi- and multilayer TFT channel structures with a high carrier mobility and high stability of the operating characteristics. The authors of [10] synthesized a transparent TFT channel material by forming ZnO and Al_2O_3 layers using atomic layer deposition (ALD). The characteristics of a transistor with pure ZnO and ZnO/Al_2O_3 multilayer channel materials were compared. It was found that the ZnO/Al_2O_3 multilayer with a total thickness of ~22 nm used as a TFT channel exhibits electrical properties better than those of ZnO. This improvement was attributed to the directed growth of ZnO crystallites with the *c* axis perpendicular to the multilayer growth front caused by the embedding of Al_2O_3 spacers, which is accompanied by an increase in the carrier mobility in the ZnO layers.

In this study, we investigate the structure and physical properties of $(ZnO/SiO_2)_{25}$ multilayer thin-film systems consisting of 25 ZnO/SiO_2 bilayers and the effect of heat treatment on the stability of the multilayer structure and its electrical properties.

2. EXPERIMENTAL

The $(ZnO/SiO_2)_{25}$ thin films were synthesized by the ion-beam sputtering of ZnO and SiO_2 ceramic targets in an argon atmosphere (99.998%) at a pressure of 7×10^{-4} Torr according to the procedure described in [11]. The targets were mounted on water-cooled copper substrates and placed in different sputtering positions in the vacuum chamber. To implement layer-by-layer deposition, the substrate was moved from one sputtering position to another by rotating the substrate holder around the axis of the sputtering chamber. Deposition was carried out onto single-crystal silicon substrates with the (100) crystallographic orientation for structural investigations and glass substrates for studying the electrical properties. During deposition, the substrates were kept at room temperature. In order to obtain different ZnO and SiO_2 thicknesses, a *V*-shaped screen was set between the target and the substrate holder during a single deposition process. The substrate holder was rotated at a speed of 0.13 rpm for the $(ZnO/SiO_2)_{25}$ films.

The layer thickness was estimated using separate ZnO and SiO_2 films preliminary deposited at preselected process parameters for depositing multilayer structure. The film thickness was measured with an MII-4 optical interferometer. Knowing the number of revolutions of the substrate holder, we calculated the film thickness obtained for one passage of the substrate through the material deposition zone, i.e., the thickness of a single layer of one of the deposited oxides. The thickness of a single layer of the second phase of the multilayer structure was determined similarly.

The number of revolutions of the substrate holder specified the number of bilayers in the $(ZnO/SiO_2)_{25}$ multilayer film. Using the described technique, 25 bilayers were formed. The bilayer thickness ranged from 7.4 to 9.6 nm; with an increase in the bilayer thickness, the ZnO-layer thickness increased from 3.9 to 6.3 nm and the SiO_2-layer thickness decreased from 3.5 to 3.2 nm. The film structure was studied by X-ray diffraction on a Bruker D2 Phaser diffractometer ($\lambda_{CuK\alpha 1} = 1.54$ Å) using the DIFFRAC.EVA 3.0 software with the ICDD PDF Release 2012 database. Cross-sectional transmission electron microscopy (TEM) study was carried out on a Hitachi HT7700 TEM with an accelerating voltage of 100 keV (*W* source). The samples were prepared using a Hitachi FB2100 focused ion beam (FIB) system (a single-beam FIB) at an accelerating voltage of 40 kV and additional finishing with low-energy Ar^+ ions. The sample thickness was ~30–40 nm. The surface of the $(ZnO/SiO_2)_{25}$ thin films was coated with an amorphous SiO layer formed by thermal deposition to protect against Ga^+-ion beam etching.

The dependences of the resistivity on the bilayer thickness and temperature were measured by the two-probe dc method using a B7-78/1 universal digital multimeter. The relative error in measuring the resistivity of the thin films was no more than 2%.

3. EXPERIMENTAL RESULTS

3.1. Structure of the Synthesized Films

Figure 1a shows the X-ray diffraction data for the $(ZnO/SiO_2)_{25}$ heterostructures. In the angular range of $2\Theta = 30°–40°$, the X-ray diffraction patterns of the $(ZnO/SiO_2)_{25}$ thin films contain one broad maximum at $2\Theta \approx 34°$ independent of the bilayer thickness. The peak position and shape are in good agreement with the position of the ZnO(002) reflection obtained under similar conditions (the upper panel in Fig. 1a) [12], which may indicate that the $(ZnO/SiO_2)_{25}$ films are nanocrystalline.

The Bragg peaks in the small-angle region are indicative of the formation of a periodic layered structure (inset in Fig. 1a). This is confirmed by TEM microphotographs of the $(ZnO/SiO_2)_{25}$ thin-film cross section (Fig. 1b). Electron diffraction study revealed amorphous SiO_2 phases indicated by a diffuse halo in the electron diffraction patterns of crystalline

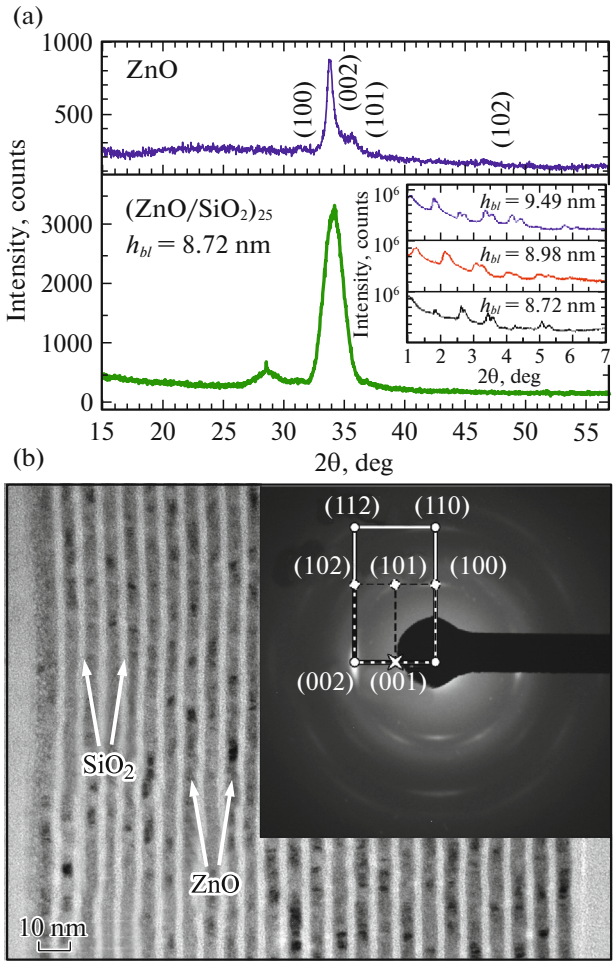

Fig. 1. (a) X-ray diffraction patterns for the ZnO thin film and $(ZnO/SiO_2)_{25}$ heterostructure with a bilayer thickness of h_{bl} = 8.72 nm (the inset shows the X-ray diffraction patterns of the $(ZnO/SiO_2)_{25}$ heterostructures with different bilayer thicknesses measured in the region of small Bragg angles). (b) TEM microphotograph of the cross section and electron diffraction pattern for the $(ZnO/SiO_2)_{25}$ thin film with h_{bl} = 7.76 nm.

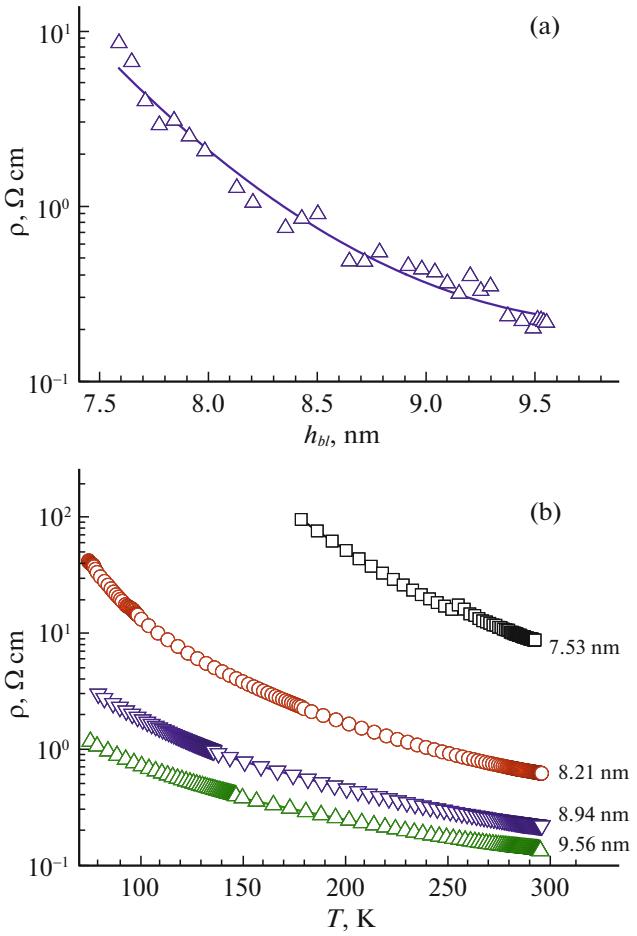

Fig. 2. Resistivity ρ of the $(ZnO/SiO_2)_{25}$ thin-film heterostructures measured at T = 300 K on (a) the bilayer thickness h_{bl} and (b) the temperature.

ZnO, which can be observed as arched reflections (inset in Fig. 1b). Based on analysis of the high-resolution microphotographs and electron diffraction patterns, we can conclude that the ZnO spacers are nanocrystalline. According to the electron diffraction patterns, the layers contain crystallites with two orientations described by the relation (100)[001] ∥ (110)[001]; the (001) axes of ZnO nanograins are perpendicular to the layer planes in the multilayer structure. It should be noted that the arrangement of the layers relative to the substrate plane is somewhat misoriented, which manifests itself as blurring of the electron diffraction reflections.

Thus, the $(ZnO/SiO_2)_{25}$ thin film structure is a multilayer system with nanocrystalline ZnO layers separated by amorphous SiO_2 layers and the ZnO in the layers has a strong texture with the ⟨001⟩ axis.

3.2. Electrical Properties of the Synthesized Films

Figure 2 presents the measured resistivity of the synthesized structure as a function of the bilayer thickness h_{bl}. Measurements of the resistivity in an electric field applied parallel to the layer plane showed that the conductivity of the films increases with the bilayer thickness, which results from a slight decrease in the SiO_2 spacer thickness and an increase in the ZnO spacer thickness.

To establish the main conductivity mechanisms in the synthesized $(ZnO/SiO_2)_{25}$ films, we studied the temperature dependences of the resistivity in the temperature range of 77–300 K (Fig. 2b). It can be seen that the dependences $\rho \propto f(T)$ have a negative temperature coefficient of resistance (TCR), which is characteristic of semiconductor materials. With an

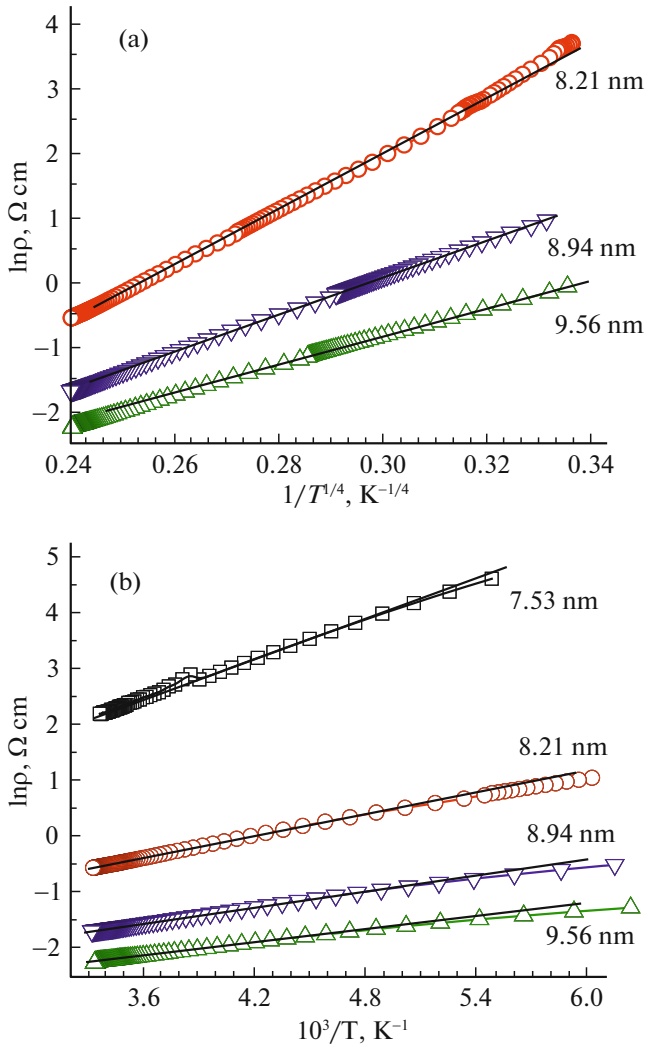

Fig. 3. Temperature dependences of the resistivity of the $(ZnO/SiO_2)_{25}$ thin films in the coordinates (a) $\ln(\rho) \propto f(T^{-1/4})$ and (b) $\ln(\rho) \propto f(1/T)$ (numerals show the bilayer thickness h_{bl}).

increase in the bilayer thickness h_{bl}, the TCR in the investigated temperature range decreases.

The obtained experimental dependences (Fig. 2b) for the $(ZnO/SiO_2)_{25}$ films were reconstructed in the coordinates $\ln(\rho) \propto f(1/T^n)$, where the exponent n took values of 1/4, 1/2, and 1, as well as $\ln(\rho) \propto f(\ln T)$ and $(\rho) \propto f(\ln(T))$. Analysis of the experimental data presented in Fig. 2b showed that, in the temperature range of 77–250 K, the resistivity is satisfactorily described by a straight line in the coordinates $\ln(\rho) \propto f(1/T^{1/4})$ (Fig. 3a), which is indicative of hopping conductivity with a variable length of hopping over localized states lying in a narrow energy band near the Fermi level. Then, according to [13], the conductivity has the form

$$\sigma = e^2 \cdot R^2 \nu_{ph} G(E_F) \exp\left(-\frac{B}{T}\right)^{1/4}, \quad (1)$$

where

$$B = \frac{16}{a^3 k_B g(E_F)}, \quad (2)$$

e is the elementary charge, R is the average hopping length, ν_{ph} is the interaction phonon-spectrum factor, T is the absolute temperature, $g(E_F)$ is the density of states at the Fermi level, a is the electron wavefunction localization radius, and k_B is the Boltzmann constant.

Knowing the electron localization radius and B value, we can estimate, using formula (2), the effective density of states at the Fermi level $g(E_F)$. Taking the electron localization radius equal to the effective Bohr radius

$$a_B = \frac{\varepsilon_0 \hbar}{m^* e^2}, \quad (3)$$

where ε_0 is the ZnO static permittivity (8.5) [14], $m^* \sim m_0$ is the effective electron mass, and e is the elementary charge. The calculation for ZnO yields $a_B \approx 0.46$ nm. The carrier hopping length for different film compositions at a temperature of 200 K is determined by the formula [13]

$$R(T) = \frac{3}{8} a B^{1/4} T^{-1/4}. \quad (4)$$

The parameters of the $(ZnO/SiO_2)_{25}$ thin films calculated from the results of processing of the data in Fig. 3a using the model of hopping conductivity over localized states at a variable hopping length are given in Table 1.

Table 1. Parameters of the $(ZnO/SiO_2)_{25}$ thin films with different bilayer thicknesses h_{bl} calculated using the model of hopping conductivity over localized states near the Fermi level in the temperature range from 80 to 250 K

h_{bl}, nm	B, K	$g(E_F)$, $eV^{-1}\,cm^{-3}$	R (200K), nm
8.21	$(44.253)^4$	4.97×10^{20}	2.03
8.94	$(28.380)^4$	2.94×10^{21}	1.3
9.56	$(21.438)^4$	9.03×10^{21}	0.98

The estimates given in Table 1 show that, with increasing bilayer thickness, the density of electronic states at the Fermi level increases. This is probably due to the fact that, as the bilayer thickness increases, the thickness of the ZnO spacers, which are mainly involved in electrotransport, grows and the SiO_2 spacer thickness decreases. Another important result of the estimation is that the obtained average hopping length is two to three times smaller than the ZnO single-layer thicknesses, which confirms the validity of formula (1) for three-dimensional hopping transport. Consequently, zinc-oxide layers and the interface

between the layers make a decisive contribution to the conductivity of the $(ZnO/SiO_2)_{25}$ thin films.

The experimental dependences of the resistivity in the temperature range of 250–300 K are linear in the coordinates $\ln(\rho) \propto f(1000/T)$ (Fig. 3b). To describe the temperature dependences of the conductivity in this range, we use the thermally activated conductivity model; then, according to [13], the resistivity should be

$$\rho = \rho_0 \exp\left(-\frac{W}{k_B T}\right), \quad (5)$$

where W is the conductivity activation energy. Using formula (5), we estimate the conductivity activation energy from Fig. 3b. The estimates are given in Table 2.

The obtained W data correspond to the levels of Zn interstitials, which are shallow donors in the ZnO films [15]. Thus, the conductivity of the $(ZnO/SiO_2)_{25}$ thin films at temperatures close to room temperature can be considered impurity-type, i.e., determined by the impurity levels of the zinc-oxide spacers.

3.3. Effect of Heat Treatment on the Structure and Electrical Properties of $(ZnO/SiO_2)_{25}$ Films

To establish the effect of heat treatment on the structure and electrical properties of the $(ZnO/SiO_2)_{25}$ thin films, we studied the temperature dependences of the resistivity in the temperature range from room temperature to 600°C in vacuum at a residual gas pressure of $P = 5 \times 10^{-4}$ Torr. Figure 4 shows the temperature dependence of the resistivity for the $(ZnO/SiO_2)_{25}$ thin films with a bilayer thickness of $h_{bl} = 7.65$ and 9.56 nm (curves *1* and *2*, respectively) upon heating to 600°C and subsequent cooling. Upon heating above room temperature, the resistivity of the samples decreases and takes its minimum value at a temperature of ~300°C. Above this temperature, the resistivity of the sample starts growing, while the most intense growth in the resistivity is observed at 580°C for the films with a thickness of $h_{bl} = 7.65$ nm and at 530°C for the sample with $h_{bl} = 9.56$ nm. The $\rho(T)$ dependences measured upon cooling have a positive TCR typical of semiconductor materials; the resistivity of the $(ZnO/SiO_2)_{25}$ thin films with a bilayer thickness of $h_{bl} = 9.56$ nm (curve *2*) became larger than the resistivity of the $(ZnO/SiO_2)_{25}$ thin films with $h_{bl} = 7.65$ nm (curve *1*).

To explain the above-described $\rho(T)$ dependences, we analyze the structure and phase composition of the $(ZnO/SiO_2)_{25}$ thin films subjected to heat treatment. Figure 5 presents X-ray diffraction patterns of the $(ZnO/SiO_2)_{25}$ multilayer structure with a bilayer thickness of $h_{bl} = 9.21$ nm after heat treatment in a vacuum chamber with a residual pressure of $P = 5 \times 10^{-4}$ Torr and different temperatures. The presented in Fig. 5a $I(2\Theta)$ dependences measured in the small Bragg angle range

Table 2. Energies of activation of the conductivity W for $(ZnO/SiO_2)_{25}$ thin films in the temperature range of 250–300 K

h_{bl}, nm	W, eV
7.53	0.110 ± 0.020
8.21	0.053 ± 0.008
9.56	0.040 ± 0.007
8.94	0.032 ± 0.005

of $2\Theta < 7°$ show that heat treatment in vacuum at temperatures below 500°C does not lead to destruction of the multilayer, although the reflections begin to slightly broaden, which can be interpreted as a slight blurring of the interfaces due to mutual diffusion of the layer materials. The stability of the nanostructured state against heat treatment at temperatures of $T <$ 500°C is confirmed also by investigations in the angle range of $2\Theta = 24–45°$. The average ZnO crystallite size was estimated using the Scherrer formula [16]

$$D = \frac{0.89\lambda}{b\cos\Theta}, \quad (6)$$

where λ is the X-ray wavelength (1.54 Å for CuK_α radiation), b is the reflection full width at half maximum, Θ is the Bragg angle, and D is the average crystal size. Estimation showed that heat treatment at a temperature of $T = 400$°C leads to a slight increase in the crystallite size (from 5.6 to 5.7 nm) as compared to the films in the initial state; however, an increase in the annealing temperature to $T = 500$°C caused a decrease in the crystallite size to 4.6 nm, which originates from mutual diffusion of the layer materials and the onset of

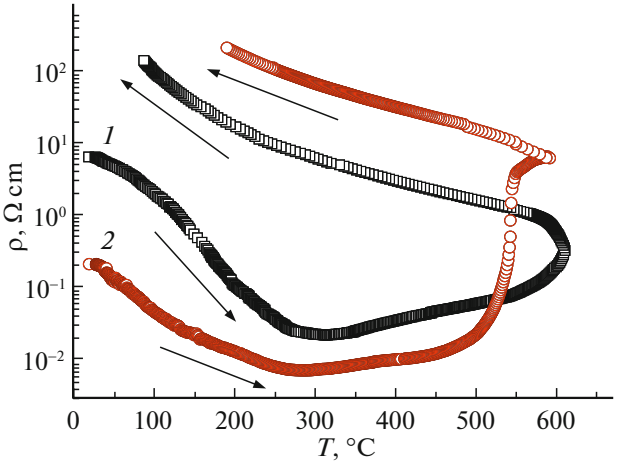

Fig. 4. Temperature dependences of the resistivity of the $(ZnO/SiO_2)_{25}$ thin films with different bilayer thicknesses h_{bl} measured in a vacuum chamber with a residual pressure of $P = 5 \times 10^{-4}$ Torr. (*1*) $h_{bl} = 7.65$ nm and (*2*) $h_{bl} = 9.56$ nm.

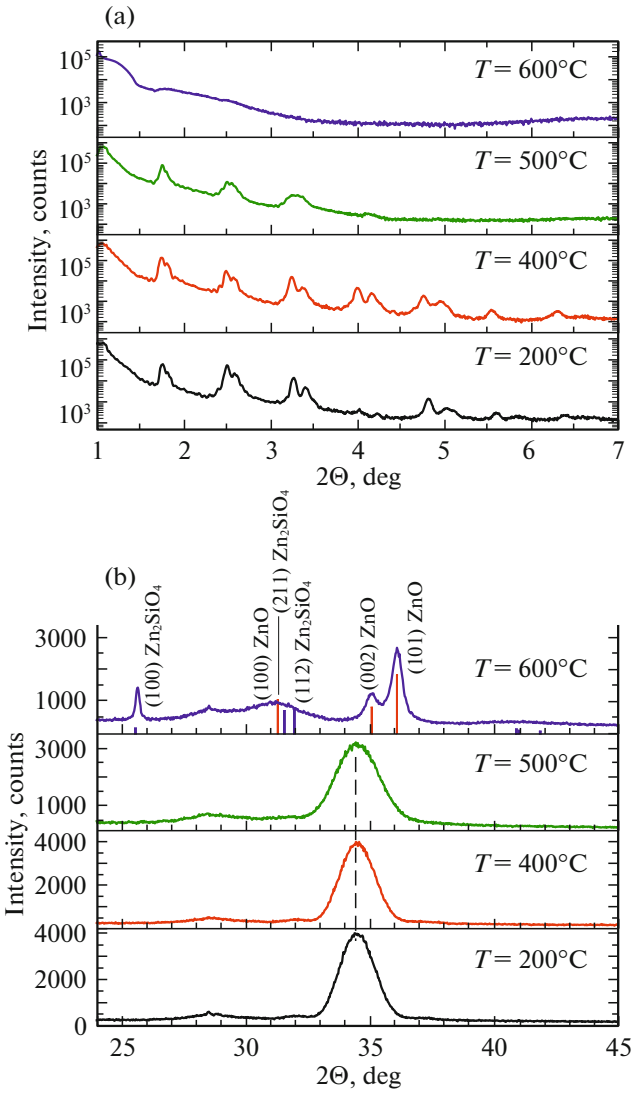

Fig. 5. X-ray diffraction patterns of the $(ZnO/SiO_2)_{25}$ thin-film heterostructures with a bilayer thickness of h_{bl} = 9.21 nm after heat treatment in a vacuum chamber with a residual pressure of $P = 5 \times 10^{-4}$ Torr and different temperatures for 30 min.

their chemical interaction. It should be noted that the thickness of the ZnO single layer in the initial sample was 5.7 nm, which is quite consistent with the estimated crystallite sizes.

An increase in the heat-treatment temperature to 600°C leads to chemical interaction between the ZnO and SiO_2 layers and formation of the Zn_2SiO_4 compound with a tetragonal structure (sp. gr. I-42*d*) (the upper panel in Fig. 5b) and to an increase in the ZnO crystal size to ~19 nm. All this leads to destruction of the multilayer structure, which is confirmed by the absence of reflections in the X-ray diffraction patterns in the region of small 2Θ values (the upper panel in Fig. 5a). The occurrence of the nonconducting Zn_2SiO_4 phase manifests itself in the growth of the resistivity of the $(ZnO/SiO_2)_{25}$ thin films after heat treatment at $T = 600$°C.

4. CONCLUSIONS

$(ZnO/SiO_2)_{25}$ multilayer thin films consisting of nanocrystalline ZnO layers and amorphous SiO_2 spacers were synthesized by ion-beam sputtering. The bilayer thickness in the obtained structures ranged from 6 to 10 nm. In the temperature range of 77–300 K, the temperature dependences of the resistivity for the synthesized films were studied. It was established that, in the $(ZnO/SiO_2)_{25}$ thin films in the investigated temperature range, the dominant conductivity mechanism successively changes from hopping with variable length in a narrow energy band near the Fermi level at nitrogen temperatures to impurity at temperatures close to room temperature. Based on the investigated temperature dependences of the resistivity, the effective density of localized states at the Fermi level and the activation energy of the impurity levels were estimated.

The effect of heat treatment in vacuum on the structure and electrical properties of the synthesized films was examined. It was found that the multilayer structure of $(ZnO/SiO_2)_{25}$ thin films is stable up to temperatures of 560–600°C, at which the ZnO and SiO_2 layers chemically interact with destruction of the multilayer structure, formation of the Zn_2SiO_4 compound with a tetragonal structure (sp. gr. I-42*d*), and growth of ZnO crystals.

ACKNOWLEDGMENTS

We are grateful to the Center of Collective Use, Krasnoyarsk Scientific Center for providing the possibility of carrying out electron microscopy investigations of the samples.

FUNDING

This study was carried out in the framework of the state assignment of the Ministry of Science and Higher Education of the Russian Federation, project no. 3.1867.2017/4.6.

CONFLICT OF INTEREST

The authors declare that they have no conflict of interest.

REFERENCES

1. D. C. Look and B. Claflin, MRS Symp. Proc. **829**, 8.6 (2005).
2. Q. Xu, L. Hartmann, H. Schmidt, H. Hochmuth, M. Lorenz, R. Schmidt-Grund, C. Sturm, D. Spemann, and M. Grundmann, Phys. Rev. B **73**, 205342 (2006).

3. T. S. Herng, S. P. Lau, C. S. Wei, L. Wang, B. C. Zhao, M. Tanemura, and Y. Akaike, Appl. Phys. Lett. **95**, 133103 (2009).
4. K. Toshio and H. Hideo, NPG Asia Mater. **2**, 15 (2010).
5. H. M. Kim, C. H. Lee, and B. Kim, J. Nanosci. Nanotechnol. **19**, 1790 (2019).
6. L. K. Markov, A. S. Pavlyuchenko, and I. P. Smirnova, Semiconductors **53**, 172 (2019).
7. S. Sanctis, J. Krausmann, and C. Guhl, J. Mater. Chem. C **6**, 464 (2018).
8. S. Nam, J. H. Yang, S. H. Cho, J. H. Choi, O. S. Kwon, E. S. Park, S. J. Lee, K. I. Cho, J. Jang, and C. S. Hwang, J. Mater. Chem. C **4**, 11298 (2016).
9. Ch. H. Ahn, S. H. Kim, Y. K. Kim, H. S. Lee, and H. K. Cho, Thin Solid Films **584**, 336 (2015).
10. G. Cui, D. Han, J. Dong, Y. Cong, X. Zhang, H. Li, W. Yu, S. Zhang, X. Zhang, and Yi. Wang, Jpn. J. Appl. Phys. **56**, 04CG03 (2017).
11. V. V. Ryl'kov, S. N. Nikolaev, V. A. Demin, A. V. Emel'yanov, A. V. Sitnikov, K. E. Nikiruy, V. A. Levanov, M. Yu. Presnyakov, A. N. Taldenkov, A. L. Vasiliev, K. Yu. Chernoglazov, A. S. Vedeneev, Yu. E. Kalinin, A. B. Granovsky, V. V. Tugushev, and A. S. Bugaev, J. Exp. Theor. Phys. **126**, 353 (2018).
12. O. V. Zhilova, S. Yu. Pankov, A. V. Sitnikov, Yu. E. Kalinin, and I. V. Babkina, AIP Conf. Proc. **1886**, 020054 (2017).
13. N. F. Mott and E. A. Davis, *Electron Procuresses in Non-Crystalline Materials* (Clarendon, Oxford, 1979; Mir, Moscow, 1982).
14. N. Ashkenov, B. N. Mbenkum, C. Bundesmann, V. Riede, M. Lorenz, D. Spemann, E. M. Kaidashev, A. Kasic, M. Schubert, and M. Grundmann, J. Appl. Phys. **93**, 126 (2003).
15. F. Oba, A. Togo, I. Tanaka, J. Paier, and G. Kresse, Phys. Rev. B **77**, 245202 (2008).
16. M. Maddahfar, M. Ramezani, and S. M. Hosseinpour-Mashkani, Appl. Phys. A **122**, 752 (2016).

Translated by E. Bondareva